Acta Astronautica 207 (2023) 316–330

Contents lists available at ScienceDirect

Acta Astronautica

journal homepage: www.elsevier.com/locate/actaastro

Time Optimal Drag-Based Targeted De-Orbiting for Low Earth Orbit

Emanuela Gaglio [a], Riccardo Bevilacqua [b,*]

[a] Cosmology, Space Science and Space Technology, Scuola Superiore Meridionale, Largo S. Marcellino 10, Naples, 80138, Italy
[b] Department of Aerospace Engineering, Embry-Riddle Aeronautical University, 1 Aerospace Boulevard, Daytona Beach, FL, 32114, United States

ARTICLE INFO

Keywords:
De-orbiting
Optimization
Minimum time

ABSTRACT

Controlled de-orbiting plays a crucial role in any space mission to ensure landing of a satellite or capsule in the desired location and preventing damage to people and property on the ground caused by debris. The necessary orbital energy reduction from the initial conditions to the re-entry interface can be achieved using a de-orbit burn or exploiting drag modulation as a control mechanism. The current work perfectly fits in this scenario, proposing a novel algorithm to generate minimum-time optimal trajectories for a satellite ballistic de-orbiting from a Low Earth Orbit (LEO) to the atmospheric re-entry interface. The formulation is written in terms of modified equinoctial orbital parameters, particularly suitable for trajectory analysis and optimization, even in cases of oscillatory problems with large time scales as in the de-orbiting problem. The optimization problem is solved with the MATLAB software GPOPS-II using a hp adaptive Gaussian quadrature orthogonal collocation method. It is formulated as a single-stage optimization problem considering the exposed surface as a control variable. The cost function to be minimized is the final time, while the imposition of an event constraint on the altitude at the de-orbit point ensures its value is in an acceptable range. A novel class of solutions is defined for the algorithm implementation to guarantee the desired values of latitude and longitude. It has been used to generate high-precision optimal trajectories and corresponding control variable laws in different conditions. The identification of a common trend of solutions along an infinite-shaped pattern allowed the possibility to model a wide range of missions, involving different initial conditions and satellites. A subsequent Monte Carlo analysis showed the algorithm validity and robustness with a successful outcome on 500 cases and an error less of 0.5% for most of them.

1. Introduction

Since the beginning of human activity in space, protecting people and properties from spacecraft-related damage has become a crucial consideration for engineers [1,2]. To ensure a satellite or capsule lands in a desired location, and to avoid debris damage to population and ground assets, a controlled de-orbiting is imperative, for both manned and unmanned space missions. In addition to protecting objects on the ground, controlled de-orbiting is also important for missions involving scientific experiments demanding the recovery of samples for further analysis (e.g., biological samples, medical monitoring equipment, pharmaceutical testing).

A typical re-entry scenario consists of two phases: the de-orbiting, from the initial conditions to the atmospheric re-entry interface, and a final stage, ending at the desired landing point. The primary topic of this research is the de-orbiting phase. In most of the existing literature, the focus is on satellite de-orbiting performed using a de-orbit burn, which is based on the application of thrust in an opposite direction with respect to the satellite motion to reduce the orbital speed and subsequently lower the orbit. An alternative de-orbiting control mechanism is drag modulation, which exploits atmospheric drag variation to achieve the necessary orbital energy reduction from the initial condition to the re-entry interface. Some technological solutions include the employment of retractable tape-spring booms [3,4] or mechanisms able to modulate the drag by varying the aerodynamic shape of the spacecraft [5–8].

For any de-orbiting technique, it is extremely important for the satellite to reach the de-orbiting point with high precision to ensure the landing point is positioned within a specific region. In literature, several works investigate the employment of drag for attitude control [9–11], satellite maneuvering [12–14], formation flight and constellation maintenance [15–22]. However, a limited number of them involves the use of aerodynamic drag to achieve a controlled de-orbit [23–27]. In Ref. [23], drag modulation is the control mechanism used to de-orbit. The algorithm is based on an analytical solution to determine the ballistic coefficient law necessary to reach a desired de-orbiting point. The

* Corresponding author.
E-mail address: bevilacr@erau.edu (R. Bevilacqua).

https://doi.org/10.1016/j.actaastro.2023.03.011
Received 8 March 2023; Accepted 9 March 2023
Available online 11 March 2023

Nomenclature

a	Semi-major axis
C_D	Drag coefficient
e	Eccentricity
f, g	Modified equinoctial parameters related to eccentricity
h, k	Modified equinoctial parameters related to inclination
J_k	kth zonal gravity coefficient
H	Altitude
i	Orbital inclination
L	True longitude
m	Mass
p	First modified equinoctial parameter
P_k	kth order Legendre polynomial
r	Geocentric position of satellite
R_e	Radius of Earth
S	Exposed surface
θ	True anomaly
Φ	Geocentric latitude
ω	Argument of perigee
ω_e	Earth angular velocity
Ω	Right ascension of ascending node
μ	Gravitational parameter
ρ	Atmospheric density
∞_S	Set of optimal control problem solutions for a fixed final true longitude

use of an analytical exponential model for density, not considering possible fluctuations, and the application on only circular orbits make the simulated problems less realistic. Also, in Refs. [24–26] the work exploits the modulation of the ballistic coefficient to reach a desired de-orbiting point. A trajectory is generated in which the spacecraft maintains a certain ballistic coefficient C_{b1} until a time t_{swap}, C_{b2} until t_{term}, and C_{btem} until the de-orbiting point, fixed at an altitude of 70 km. The adopted procedure is based on the estimation of the control parameters, C_{b1}, C_{b2}, and t_{swap} to reduce the final error between the desired and the evaluated de-orbiting point. However, this procedure only attempts to minimize the final error on the de-orbiting point without considering the maneuver duration.

In [27], the ballistic coefficient profile to guarantee landing in a specific location is generated using the optimization tool by NASA: Program to Optimize Simulated Trajectories II. However, this algorithm is characterized by some weaknesses including the lack of convergence and performance in some cases. Additionally, the optimizer is not tuned to the specific problem. The work proposed here perfectly fits in this scenario, proposing a novel minimum-time optimization algorithm for a ballistic de-orbiting from a Low Earth Orbit (LEO) to the re-entry interface. The formulation is written in terms of modified equinoctial parameters [28–30], which results particularly suitable in cases of trajectory analysis and optimization, even in the case of large time scales. This formulation has been widely used in different scenarios [31–36] but has yet to be utilized for a de-orbiting scenario until this work. The optimization problem is solved with the software GPOPS-II [37,38] using an hp adaptive Gaussian quadrature orthogonal collocation method [37–40]. The goal is to get minimum-time de-orbiting trajectories ensuring desired values of altitude, latitude, and longitude at the re-entry interface with high accuracy. The problem is formulated as a single-stage optimization, considering the exposed surface of the re-entry object as the control variable. The cost function to be minimized is the final time while the desired final altitude is guaranteed by defining an event constraint to impose its value in an acceptable range. The latitude and longitude values are not directly imposed in the optimization problem, but a novel algorithm is implemented to find the optimal control problem parameters, in particular the final value of true longitude and the number of its cycles, which ensure the desired values. An intelligent initial guess of the solution is considered, solving the de-orbiting problem for a constant intermediate value of the control parameter.

As a conclusion, this work provides a novel optimization algorithm able to get minimum-time de-orbiting trajectories from different possible initial conditions to a desired point at the re-entry interface. The identification of a common trend of solutions along an infinite-shaped pattern allows the possibility to model a wide range of missions, involving different initial conditions and satellites.

Section 2 describes the minimum-time optimal control problem formulation, explaining the equations of the dynamics, the boundary conditions, the cost function, and the initial guess generation. Section 3 focuses on the novel algorithm to assess the optimal control problem parameters that guarantee the desired values of latitude and longitude. Section 4 presents the algorithm results when applied in different cases and discussion of the results, while Section 5 provides the main conclusions of the work.

2. Optimal control problem formulation

The goal of this research is to obtain minimum-time de-orbiting trajectories for a satellite de-orbiting from a Low Earth Orbit (LEO) to a desired re-entry interface point, producing the desired altitude, latitude, and longitude values at the re-entry interface with high accuracy. The problem is formulated as a single-stage optimization, based on a hp adaptive Gaussian quadrature orthogonal collocation method [37–40] and is solved with the MATLAB software GPOPS-II [37,38], considering the exposed surface of the de-orbiting object as the control variable.

2.1. Dynamics equations

The dynamics of the problem is described in terms of modified equinoctial orbital parameters (p, f, g h, k, L), particularly useful for trajectories analysis and optimization [28–30]. They are related to the classical ones by the following equations:

$$p = a\left(1 - e^2\right) \tag{1}$$

$$f = e\cos\left(\omega + \Omega\right) \tag{2}$$

$$g = e\sin\left(\omega + \Omega\right) \tag{3}$$

$$h = \tan\left(i/2\right)\cos\Omega \tag{4}$$

$$k = \tan\left(i/2\right)\sin\Omega \tag{5}$$

$$L = \Omega + \omega + \theta \tag{6}$$

where L is the true longitude, representing a parameter of interest in the current optimization algorithm. Its definition refers to a fixed direction, the First Point of Aries, implying its value repetition after $2\pi n$, where n is an integer. The differential equations of motion of the orbiting satellite are given by the following:

$$\dot{p} = \frac{dp}{dt} = \frac{2p}{w}\sqrt{\frac{p}{\mu}}\Delta_t \tag{7}$$

$$\dot{f} = \frac{df}{dt} = \sqrt{\frac{p}{\mu}}\left[\Delta_r \sin L + \left[(w+1)\cos L + f\right]\frac{\Delta_t}{w} - (h\sin L - k\cos L)\frac{g\Delta_n}{w}\right] \tag{8}$$

$$\dot{g} = \frac{dg}{dt} = \sqrt{\frac{p}{\mu}}\left[-\Delta_r \cos L + [(w+1)\sin L + g]\frac{\Delta_t}{w} + (h \sin L - k \cos L)\frac{g\Delta_n}{w}\right] \tag{9}$$

$$\dot{h} = \frac{dh}{dt} = \sqrt{\frac{p}{\mu}}\frac{s^2\Delta_n}{2w}\cos L \tag{10}$$

$$\dot{k} = \frac{dk}{dt} = \sqrt{\frac{p}{\mu}}\frac{s^2\Delta_n}{2w}\sin L \tag{11}$$

$$\dot{L} = \frac{dL}{dt} = \sqrt{\mu p}\left(\frac{w}{p}\right)^2 + \frac{1}{w}\sqrt{\frac{p}{\mu}}(h \sin L - k \cos L)\Delta_n \tag{12}$$

where:

$$w = 1 + f \cos L + g \sin L \tag{13}$$

$$r = \frac{p}{w} \tag{14}$$

$$\alpha^2 = h^2 - k^2 \tag{15}$$

$$s = \sqrt{1 + h^2 + k^2} \tag{16}$$

A change of independent variable from time to true longitude is applied to reduce computational cost. This solution has been considered also in other similar optimization problems with large time scales [33, 36]. The terms Δ_r, Δ_t and Δ_n are the non-two body perturbations in radial, tangential, and normal directions. The first one is directed along the geocentric radius vector of the satellite measured positively away from the geo-center. The tangential direction is perpendicular to the radius vector and is defined as positive in the orbital motion direction. The normal direction is positive along the angular momentum vector of the satellite orbit. The overall acceleration term, Δ, is modelled as:

$$\Delta = \Delta_g + \Delta_D \tag{17}$$

where Δ_g and Δ_D are the gravitational acceleration due to Earth oblateness and the contribution due to aerodynamic drag respectively. In relation to the first term, the non-spherical gravitational acceleration can be expressed as:

$$g = g_N \hat{i}_N - g_r \hat{i}_r \tag{18}$$

where:

$$\hat{i}_N = \frac{\hat{e}_N - (\hat{e}_N^T \hat{i}_r)\hat{i}_r}{\|\hat{e}_N - (\hat{e}_N^T \hat{i}_r)\hat{i}_r\|} \tag{19}$$

And

$$\hat{e}_N = [0 \quad 0 \quad 1]^T \tag{20}$$

with the subscript N identifying the local north direction while r the radial one. The contributions due to the zonal gravity effects of J_2, J_3 and J_4 are given by the following formulation:

$$g_N = -\frac{\mu \cos\varphi}{r^2}\sum_{k=2}^{4}\left(\frac{R_e}{r}\right)^k P_k' J_k \tag{21}$$

$$g_r = -\frac{\mu}{r^2}\sum_{k=2}^{4}(k+1)\left(\frac{R_e}{r}\right)^k P_k J_k \tag{22}$$

where μ is the gravitational parameter, r the geocentric distance of the satellite, R_e is the equatorial radius of the Earth, φ the geocentric latitude, J_k the zonal gravity coefficient, and P_k is the kth order Legendre polynomial. Therefore, the acceleration due to Earth's oblateness in rotating coordinates is:

$$\Delta_g = Q^T g \tag{23}$$

where Q is the transformation matrix between rotating and Earth Centered Inertial (ECI) coordinates. Its columns are respectively defined as:

$$\left[i_r = \frac{r}{\|r\|}, i_t = i_n \times i_r, i_n = \frac{r \times v}{\|r \times v\|}\right] \tag{24}$$

A similar approach is followed for the aerodynamic drag acceleration term Δ_D, which has been modelled as:

$$\Delta_D = Q^T a_d \tag{25}$$

where a_d is the acceleration due to drag in the ECI reference frame and is given by:

$$a_d = -\frac{1}{2m}\rho S C_D v^2 \tag{26}$$

in which m is the mass of the satellite, ρ is the atmospheric density, C_D is the drag coefficient and v is the spacecraft to atmosphere relative velocity, defined considering the atmosphere rigid and rotating with the Earth:

$$v = V - \omega_e \times r \tag{27}$$

where ω_e is the angular velocity of the Earth. In the optimal control problem formulation, the control variable is the exposed surface, S, which can be modulated to minimize the cost function. The atmospheric density has been modelled as exponential, considering the altitude variation, to reduce the computational cost of simulations. However, the case analyzed in paragraph 4.2 has been solved considering the density model NRLMSISE-00, showing a successful outcome even in this case.

2.2. Optimal control problem setting

The initial conditions of the problem are defined in terms of classical orbital elements $(a, e, i, \Omega, \omega, \theta)$ and then transformed into equinoctial ones with equations (1–6). The final values of the state variables are free, except for the true longitude for which a specific value is imposed, resulting from the algorithm explained in section 3. In the optimal control problem, the final time is defined as the terminal cost function to be minimized:

$$J = t_f \tag{28}$$

To ensure the satellite reaches a desired de-orbiting point, different conditions are imposed on the altitude, latitude, and longitude. The definition of an event constraint on the altitude guarantees its value is within an acceptable range. It is defined as:

$$H = r - R_e \tag{29}$$

with its value constrained in the interval [101 km, 103 km], acceptable for a de-orbiting point on the re-entry interface. The application of the proposed algorithm guarantees the desired final values of latitude and longitude. It attempts to define the optimal control problem parameters, particularly the final true longitude and the number of its complete cycles, to obtain the desired latitude and longitude values.

The optimal control problem is based on an intelligent initial guess of the solution, relying on the analytical solution of the problem with an intermediate value of the control variable.

3. Algorithm description

This section describes the algorithm to find the optimal control problem parameters guaranteeing the desired latitude and longitude at the de-orbiting point. They rely on the final value of true longitude and its complete cycles. The algorithm is based on the definition of a

specified final date chosen by user at which the satellite is required to reach the desired de-orbiting point. The subsequent de-orbiting time assessment allows the evaluation of the corresponding initial date. The following subsections describe the steps leading to the final definition of the complete algorithm.

3.1. Class of solutions

The oscillatory nature and the non-continuity of latitude and longitude during de-orbiting have not made it possible for their direct implementation in the cost function of the optimal control problem. Therefore, an alternative approach was found to guarantee their values remain in a desired range. To that aim, a parametric analysis has been completed to solve the optimal control problem, using the initial conditions provided in Table 1, for different values of final true longitude and its complete cycles, resulting in the class of solutions in Fig. 1. The complete cycles of true longitude identify the number of times its value is repeated from the first solution, where the control variable value is almost the maximum, to the final one. It is possible to estimate the complete cycles interval by carrying out analytical simulations with the highest and lowest values of the control variable, which is the exposed surface S in the current case.

The evolution of the resulting latitude-longitude pairs is represented by varying the final true longitude and its complete cycles. Each curve results from the optimal control problem solution for a fixed value of final true longitude and a variable number of cycles, increasing towards the direction of the black arrows. The solutions are characterized by latitude values between negative inclination and positive inclination accordingly. The longitude can achieve values between 0° and 360° and exhibits an increasing trend with true longitude, as identified by the vertical grey arrow to the right of the graph. In fact, each curve refers to a specific final value of true longitude, increasing with the direction of the grey arrow in Fig. 1. Once a desired de-orbit latitude-longitude pair is identified, only a finite number of curves can give a solution. Consequently, the search area for the final true longitude of the solution is obtained.

3.2. Influence of the Right Ascension of Ascending Node on the solution

This paragraph discusses the effect of different initial values of the Right Ascension of Ascending Node, Ω, on the solution. To this aim, optimal simulations are computed considering the initial conditions in Table 1, with the exception of Ω, varying in the range [50°, 350°]. The final fixed value of true longitude has been randomly chosen to be 121°. Fig. 2 represents the evolution of latitude-longitude optimal pairs for the different initial values of Ω. A combination of all curves in the same graph is also reported in Fig. 2 (h).

The combination of all the solutions (Fig. 2 (h)) results in an infinite-like shape, from now on defined as ∞_S, centered at a latitude of 0° and a longitude dependent on the final value of true longitude. The same analysis has been repeated for different final values of true longitude to investigate its effect on the evolution of the optimal latitude-longitude pairs. Fig. 3 reports the ∞_S corresponding to the solutions for the following final values of true longitude: 64°, 121°, 288° and 351°. These values have been chosen to clearly demonstrate the different ∞_S in the plane, without overlapping.

Table 1
Initial conditions correspondent to the class of optimal solutions.

Initial orbital parameter	Value
a_0	6680 *km*
e_0	0.0007
i_0	51.64°
ω_0	130°
θ_0	80.8°
Ω_0	300°

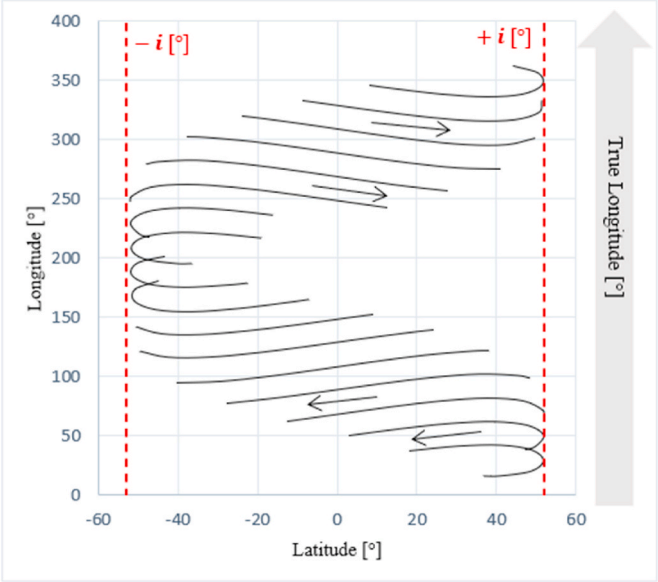

Fig. 1. Example of class of optimal solutions, for different values of final true longitude and its complete cycles.

Fig. 3 shows that different final values of true longitude correspond to a rigid translation of ∞_S in the longitude-latitude plane without changing its shape. The only differences between each case are the longitude value corresponding to the ∞_S center and the starting point, identified by the red point, representing the first solution for the lowest value of Ω. In conclusion, a different initial Ω will result in a solution motion along an ∞_S with latitude values between negative inclination and positive inclination. Different final values of true longitude correspond to a rigid vertical translation of ∞_S in the longitude-latitude plane without changing its shape.

3.3. Effect of semi-major axis on the solution

This subsection discusses the influence of the semi-major axis, a, on the solution. Following the previous approach, optimal solutions are computed considering the initial conditions in Table 1 for a fixed final true longitude, randomly chosen to be 60°, and a variable semi-major axis. Fig. 4 compares the different solutions, with the black arrows identifying the increasing values of true longitude cycles.

The graphs in Fig. 4 highlight a similar trend as seen when observing Ω. In fact, because of semi-major axis variations, the solution will move along an ∞_S centered at a latitude of 0°, exhibiting values between negative inclination and positive inclination. Additionally, the greater the semi-major axis a, the higher the number of feasible longitude-latitude couples, as shown in Fig. 4(a–c). Since the latitude and longitude upper and lower bounds do not change, the ∞_S shape and dimensions of the result are not affected by semi-major axis.

3.4. Effect of orbital inclination on the solution

This paragraph investigates the effect of orbital inclination, i, on the optimal control problem solution. To this aim, optimal solutions are computed considering the initial conditions in Table 1, fixing a final value of true longitude of 60°, and varying both Ω and i to investigate the influence of i on the ∞_S. Fig. 5 represents the corresponding evolution of the solutions. The ∞_S result uniformly scales with the latitude values between negative inclination and positive inclination while the center position is not affected. The Δ parameter represents the interval of longitude values corresponding to a specific value of orbital inclination. It exhibits a parabolic trend with the inclination starting from 0° for an

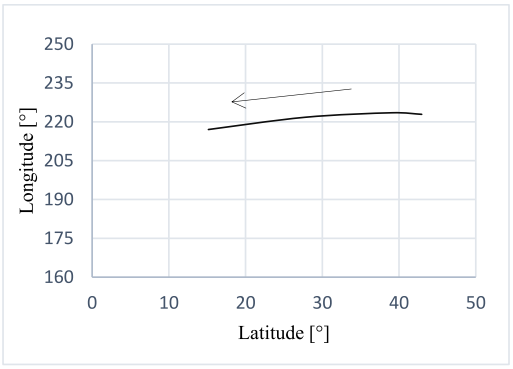

(a) $\Omega = 50°$

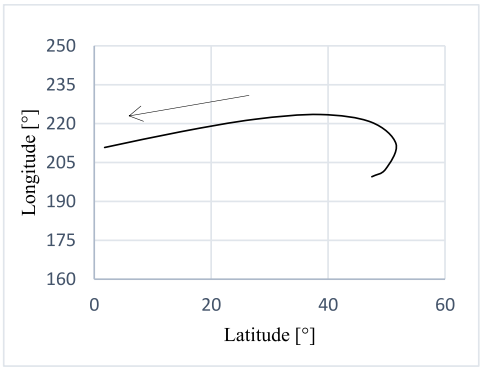

(b) $\Omega = 100°$

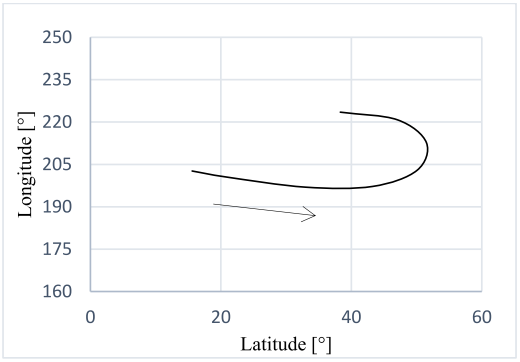

(c) $\Omega = 150°$

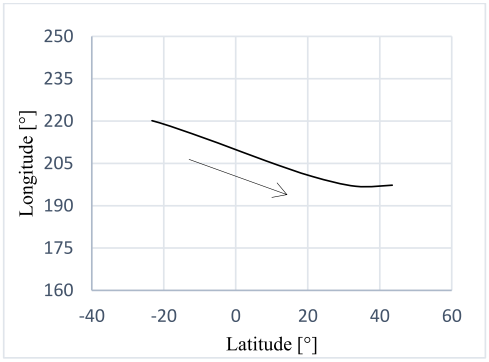

(d) $\Omega = 200°$

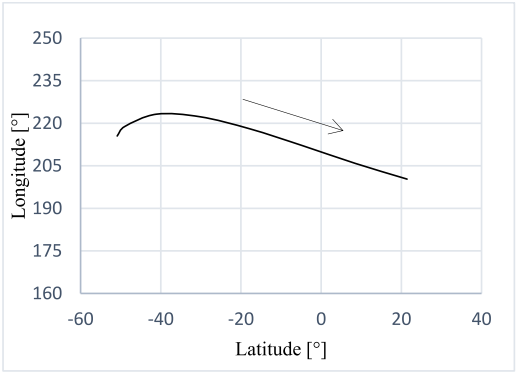

(e) $\Omega = 250°$

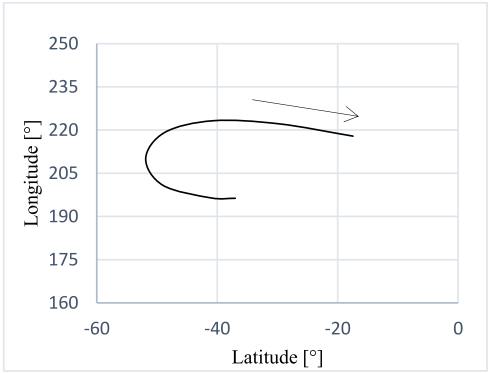

(f) $\Omega = 300°$

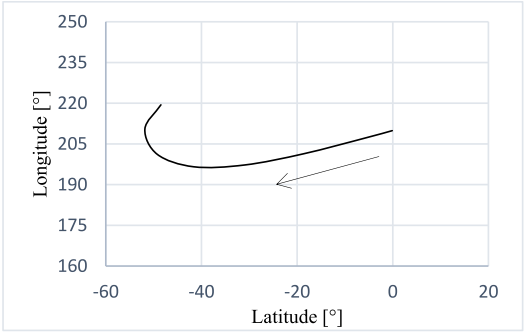

(g) $\Omega = 350°$

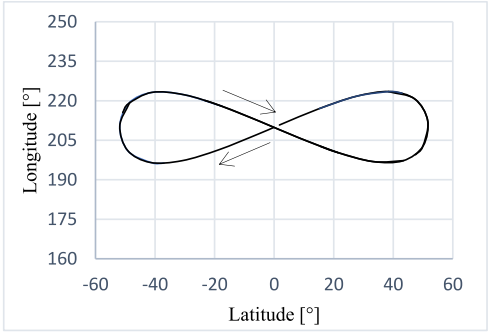

(h) Combination of all curves

Fig. 2. Evolution of the optimal control problem solution as function of $\boldsymbol{\Omega}$.

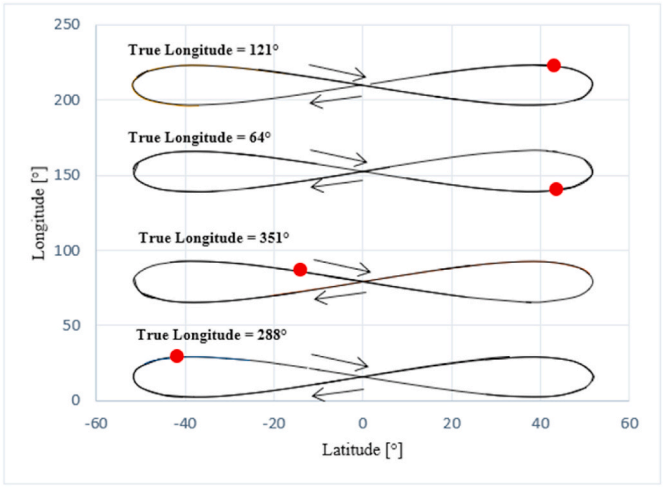

Fig. 3. Evolution of the optimal control problem solution as function of $\boldsymbol{\Omega}$, for variable values of final true longitude.

equatorial orbit, as shown in Fig. 6. Therefore, it can be estimated using only the knowledge of orbital inclination without carrying out the simulations.

As a result, a change in orbital inclination will only affect the dimensions of ∞_S but not its center position. The latter can be evaluated by carrying out an optimal control simulation for an equatorial orbit, varying the final true longitude values between 0° and 360°. Fig. 7 provides the ∞_S centers trend in the true longitude-longitude plane, where the jump occurring at x_0 represents the condition in which the longitude passes from 360° to 0° again. The graph shows a linear trend, with a unitary angular coefficient and known term q equal to the longitude at the de-orbit point, evaluated for an equatorial orbit at 0° value of true longitude. The second part of the curve is also linear with unitary angular coefficient and starting from x_0. In this graph, the inclination effect will result in two parallel lines shifted by a quantity equal to $\frac{\Delta}{2}$ referring to the main line, corresponding to the center position. Therefore, once the desired longitude value at the re-entry interface is chosen, it is possible to get an estimation of the solution's true longitude interval range. The bounds of the interval can be evaluated by looking at the intersection of the two dashed lines with the desired longitude value.

3.5. *Effect of different final date on the solution*

This section describes the effect of the final date on the results. To this aim, the graph in Fig. 7 is recreated, varying each term of the final date in Coordinated Universal Time (UTC), as year, month, day, hour,

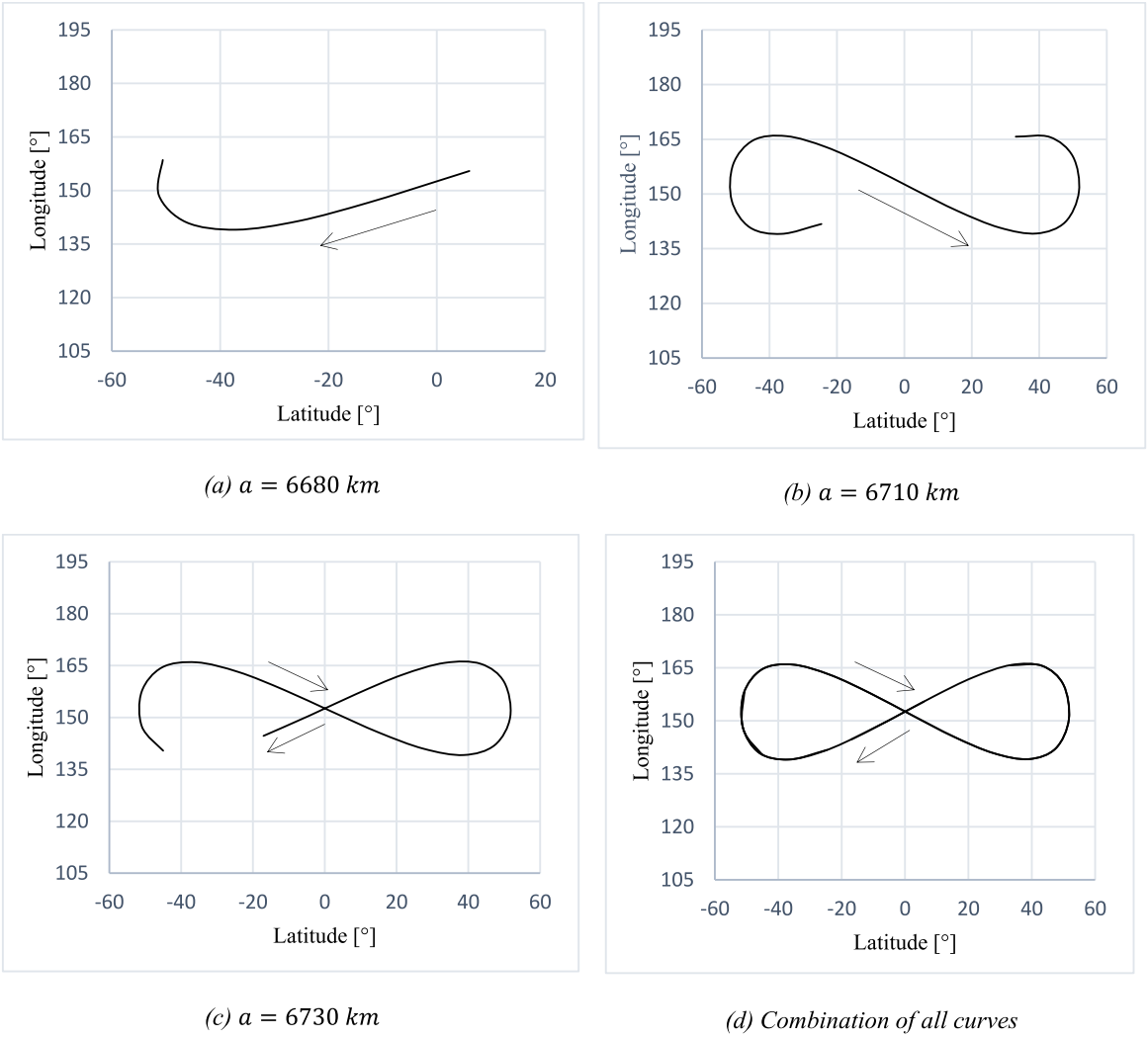

(a) $a = 6680\ km$ *(b)* $a = 6710\ km$

(c) $a = 6730\ km$ *(d) Combination of all curves*

Fig. 4. Evolution of optimal control problem solution as function of semi-major axis $\boldsymbol{a}$.

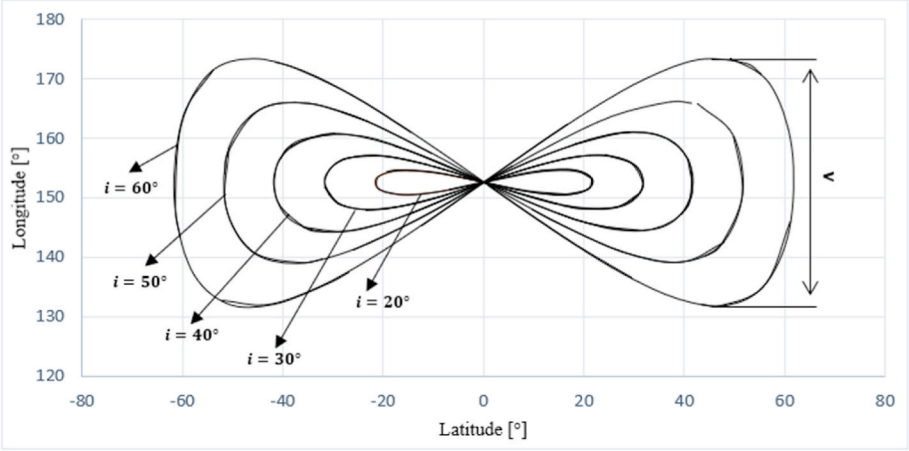

Fig. 5. Evolution of optimal control problem solution as function of orbital inclination *i*.

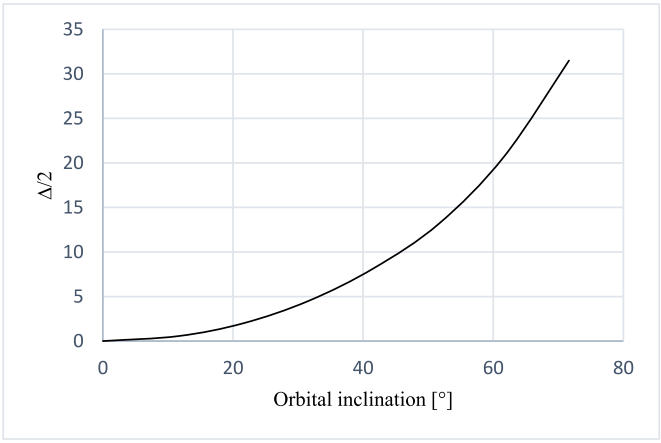

Fig. 6. Parabolic trend of $\frac{\Delta}{2}$ as function of orbital inclination *i*.

minute, and second, to investigate both their individual and combined effect on the solution. As shown in Fig. 8, a variation of each parameter results in a horizontal rigid translation of the graph, whose direction is identified by the black arrows. The final year (Fig. 8 (a)) and second (Fig. 8 (f)) have a negligible influence on the curve, a moderate effect is given by final minute (Fig. 8 (e)) and day (Fig. 8 (c)), while the greatest contribution results from a different final month (Fig. 8 (b)) and hour (Fig. 8 (d)). Table 2 summarizes the horizontal translation amount in each case. Their combination will always result in a rigid horizontal translation of the curve in the true longitude-longitude plane. As a result, the considerations made at the end of the previous paragraph are general, and the graph in Fig. 7 can be defined for any final date using a single simulation for an equatorial orbit at 0° value of true longitude, to find the intercept of the line.

3.6. Algorithm implementation

The previous analysis provided a comprehensive assessment of the influence of the different initial conditions and final date on the optimal control problem solution, summarized in Table 3.

The previous analysis led to the definition of a general algorithm to find an optimal solution, given a set of initial conditions and a specific final date. It can be summarized in the following steps:

1. Determination of true longitude cycles interval by evaluating optimal solutions with the lowest and highest value of the control variable. They will correspond to the minimum and maximum time cases.
2. With reference to Fig. 9, determination of the true longitude interval where to search for the solution with the following procedure:
   a. Simulation running for an equatorial orbit at 0° value of final true longitude, to determine the intercept *q* of the line.

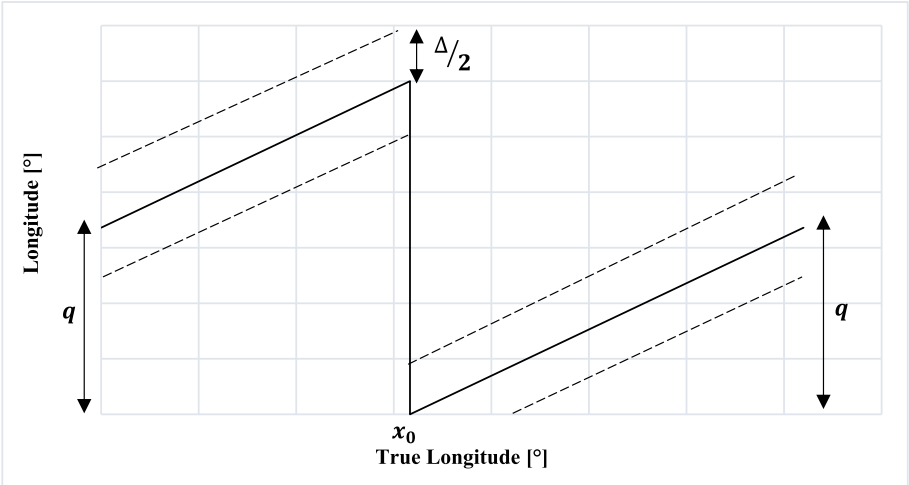

Fig. 7. Schematization of centers trend in longitude-true longitude plane, considering the effect of inclination.

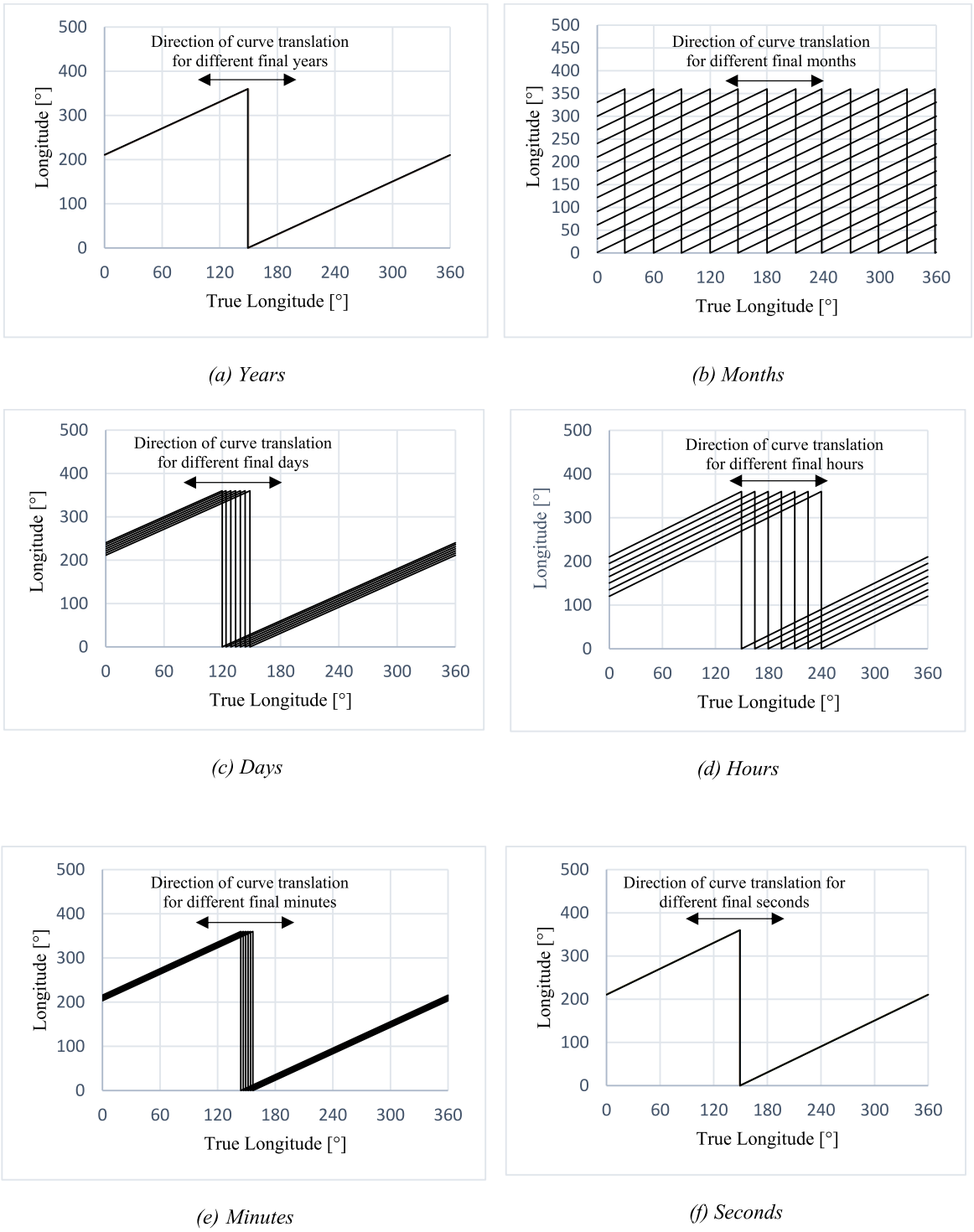

Fig. 8. Influence of a different final date.

Table 2
Horizontal rigid translation entities varying year, month, day, hour, minute and second of final date.

Date	Rigid translation amount
One year	0.25°
One month	30°
One day	5°
One hour	15°
One minute	0.25°
One second	0.0040°

b. Definition of the line equation with angular coefficient equal to 1 and intercept q as: $y = x + q$.
c. Determination of the abscissa x_0 correspondent to $y = 360°$, where the gap occurs.
d. Definition of the equation of the second part of the line, considering that the angular coefficient is the same as the first part: $y = x - x_0$.
e. Definition of lower and upper bounds $\frac{\Delta}{2}$ given by the orbital inclination. Their intersection with the line $y =$ *desired longitude*

Table 3
Summary of the influence of different parameters on the optimal control problem solution.

Parameter	Effect on the solution
Final value of true longitude	Different final values of true longitude reflect in a vertical translation of each ∞_S in the latitude-longitude plane.
Ω_0	Different values of Ω_0 correspond to a different position of the optimal curve solutions along the correspondent ∞_S.
i_0	Different values of i_0 will uniformly scale each ∞_S without changing its centre position. The Δ exhibits a parabolic trend with the inclination, starting from an equatorial orbit where the ∞_S degenerates to a point correspondent to its center.
a_0	Different values of a_0 have a similar effect as Ω_0, implying the solution curve translation along the correspondent ∞_S. In addition, the greater a_0, the higher latitude-longitude pairs possible to cover.
ω_0, θ_0, e_0	Negligible influence
Final date	Different final dates will correspond to a rigid vertical translation of ∞_S in latitude-longitude plane, without affecting its shape.

will give the true longitude interval where to search for the solution, identified by the two yellow stars in Fig. 9.

3. Using the range estimated in 2.e, start an optimization cycle with an accuracy of 10^{-4}, varying the number of complete revolutions. Start from the lowest value of the interval and compare the estimated longitude and latitude with the desired ones. Search for a possible couple of latitude and longitude respecting the threshold imposed by the user. At this point two different scenarios can occur:
   a. If the condition at point 3 is satisfied, repeat the simulation with a higher accuracy, 10^{-6}. The optimal solution has been found.
   b. If the condition at point 3 is not satisfied, repeat simulations for increasing values of true longitude until condition 3.a is satisfied.

This algorithm is valid even in cases of different masses and drag coefficients of the satellites, showing its generalization and robustness. Fig. 10 represents a block diagram of the algorithm.

4. Results

This section describes the results of the algorithm application. There are two cases studied in this research. First, a discussion on a sample case study explains the steps up to the final solution. Then, a subsequent resolution of another case comparing both the current algorithm and the one proposed in Refs. [24–26], which was not optimized. The latter highlights the ability of this algorithm to obtain a desired geolocation point at the re-entry interface in minimum time. A conclusive Monte Carlo analysis demonstrates the robustness of the algorithm and successful outcome in a wide range of conditions.

4.1. Application to a sample case study

This case study represents a mission in which a satellite de-orbits from a Low Earth Orbit (LEO) with the simulation conditions summarized in Table 4. The desired de-orbit point occurs at an altitude value of 102 km, a latitude of 30.4°, and a longitude of 29.84°. The final epoch has been fixed on 30/06/2022 at 08:15:00 UTC.

The estimated intercept q is 30.39°, resulting from the solution for an equatorial orbit at a zero final value of true longitude. The Δ value, and the correspondent dashed lined, are evaluated using the graph in Fig. 6 for an orbital inclination of 51.84°. The intersection between the narrow lines and the desired longitude value of 29.84° in Fig. 11 produced the true longitude solution interval: [58.0°; 85.0°]. In particular, the desired value of longitude is represented by the horizontal red line, the dashed lines refer to the Δ corresponding to the orbital inclination, and the yellow stars identify the bounds of true longitude interval, in which to search for the solution. The application of the iterative procedure of point 3 from the algorithm described in subsection 3.6 determined a final value of true longitude equal to 84.0°, which lies in the range estimated previously. Figs. 12–19 provide the results of the optimal control problem, displaying the trends of the variables of interest as function of time, including a zoom to better appreciate oscillating regions.

The control variable exhibits a bang-bang-like optimal profile, seen in Fig. 12, with values varying between the upper and lower bounds of the surface. Between the fifth and the sixth day, some oscillation occurs before the surface stabilizes to its lowest value. The altitude exhibits a decreasing trend (Fig. 13 (a)) characterized by the typical de-orbiting oscillations (Fig. 13 (b)) with a change in behavior corresponding to surface variation. Something similar is observed for the velocity (Fig. 14), exhibiting an increasing trend. Parameters p (Fig. 15), f (Fig. 16), and g (Fig. 17) are characterized by an oscillatory profile with a change in behavior in correspondence with the control variable change. State variables h and k are characterized by less oscillation, seen in Figs. 18 and 19. The de-orbiting time duration is 19 days, 9 h, 25 min, and 45 s, with a corresponding initial date of 10/06/2022 at 22:49:15 UTC.

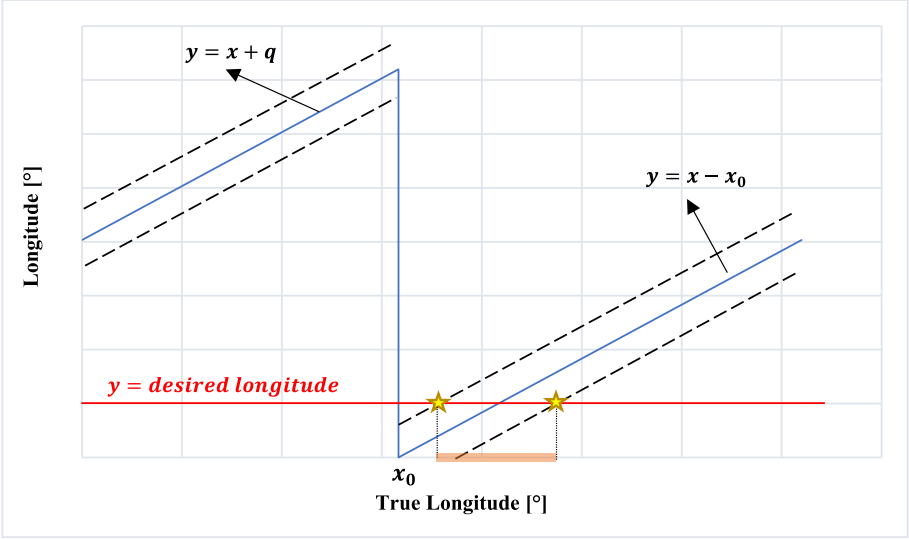

Fig. 9. Schematization of the procedure to evaluate the true longitude search interval.

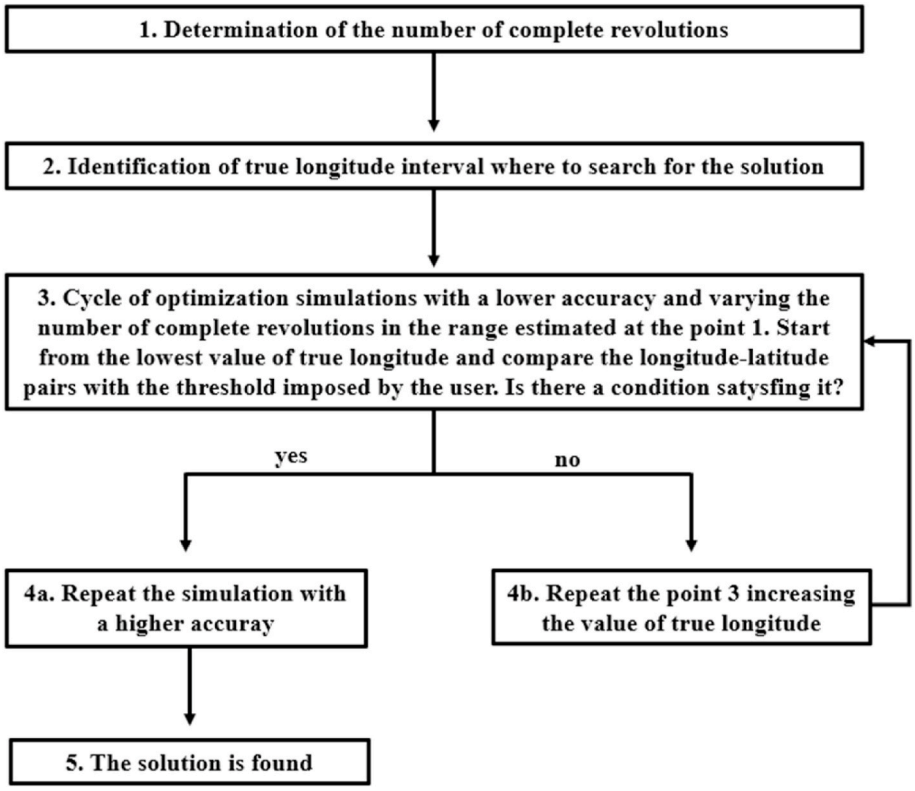

Fig. 10. Block diagram of the algorithm.

Table 4
Simulation initial conditions and satellite characteristics for the first case study.

Simulation initial conditions and satellite characteristics for the first case study	
a_0	6680 km
e_0	0.0007
i_0	51.84°
ω_0	20°
θ_0	40°
Ω_0	150°
m	40 kg
C_D	2
$[S_{min}; S_{max}]$	$[0.2\ m^2; 1.9\ m^2]$

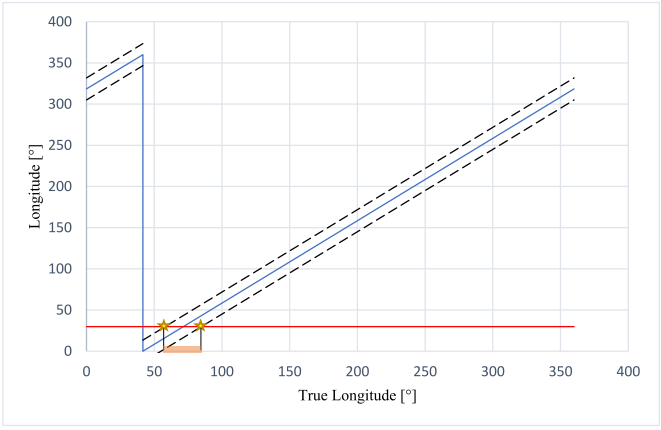

Fig. 11. Schematization of the procedure to find the true longitude search interval, applied to the sample case study.

4.2. Comparison with another de-orbiting algorithm

The ability of the algorithm to generate optimal minimum-time trajectories is further demonstrated by solving another case study and comparing the de-orbiting time with the one resulting from the application of the algorithm described in Refs. [24–26]. For consistency between the two, the density model NRLMSISE-00 is also considered in the current algorithm, despite the higher computational cost. Table 5 summarizes the initial conditions of the case study in question. About the simulation epoch, after defining the following final date, 30/01/2015 at 08:15:00 UTC, the evaluation of the corresponding initial date is calculated using the de-orbiting time, resulting from the algorithm proposed in this paper. The algorithm in Refs. [24–26], which is based on a specific initial date, has been subsequently applied to the same case study.

The application of the current algorithm results in a de-orbiting time of 10 days, 23 h, 49 min, and 7 s. The corresponding initial date evaluated is 19/01/2015 at 08:25:53 Universal Central Time (UTC). The same case study resolved with the algorithm in Refs. [24–26] results in a de-orbiting time of 17 days, 23 h, 2 min, and 47 s. In conclusion, a considerable time reduction is achieved further demonstrating the ability to get minimum-time optimal trajectories.

4.3. Monte Carlo analysis

The robustness and generalization of the algorithm are proven by its successful outcome in a wide range of scenarios, produced by a Monte Carlo analysis carried out over 500 cases. A uniform distribution of the initial mean orbital elements corresponding to a Low Earth Orbit (LEO) is considered, with an epoch range of five years. Table 6 specifies the initial conditions and parameters range, as well as their probability distributions. The maximum acceptable error has been set at 1.5%.

Fig. 20 shows the longitude-latitude pairs resulting from the Monte Carlo analysis. The light red box represents the zone where the

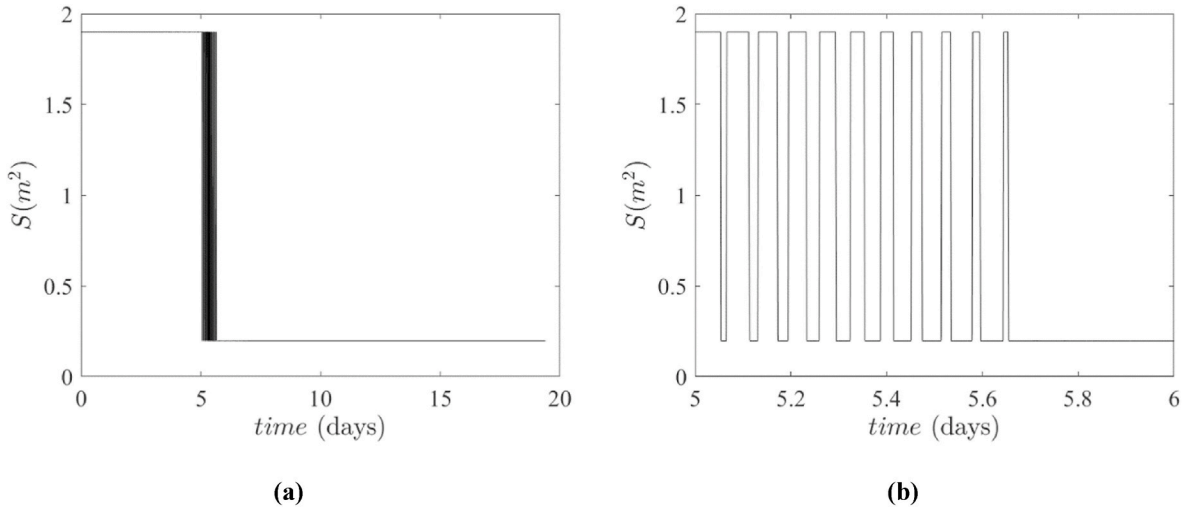

Fig. 12. Control variable profile as function of time (a), with a zoom (b) to appreciate the oscillations.

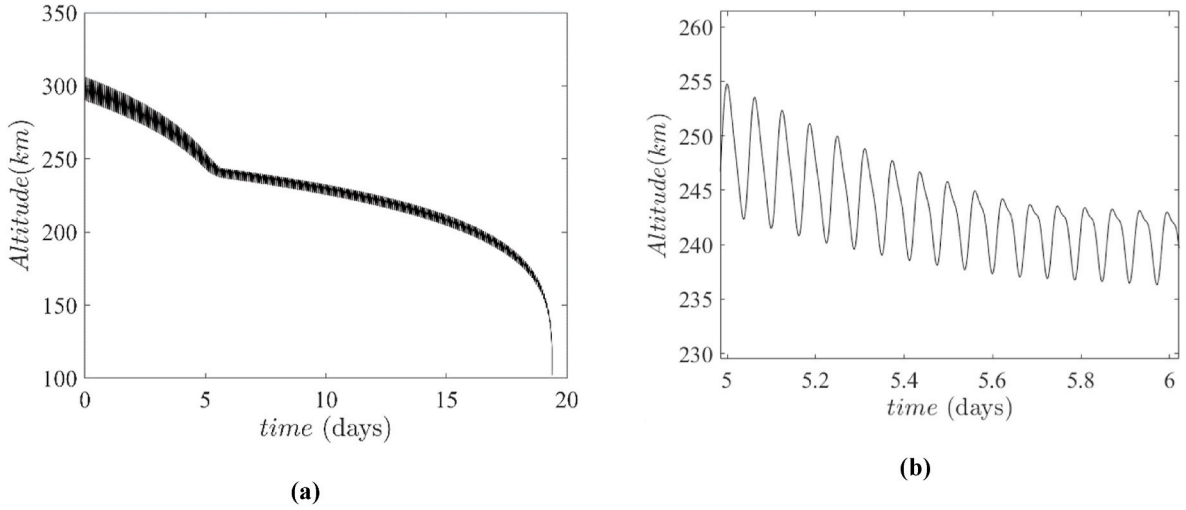

Fig. 13. Optimal profile of altitude (km) as function of time (a), with a zoom (b) to appreciate the oscillations.

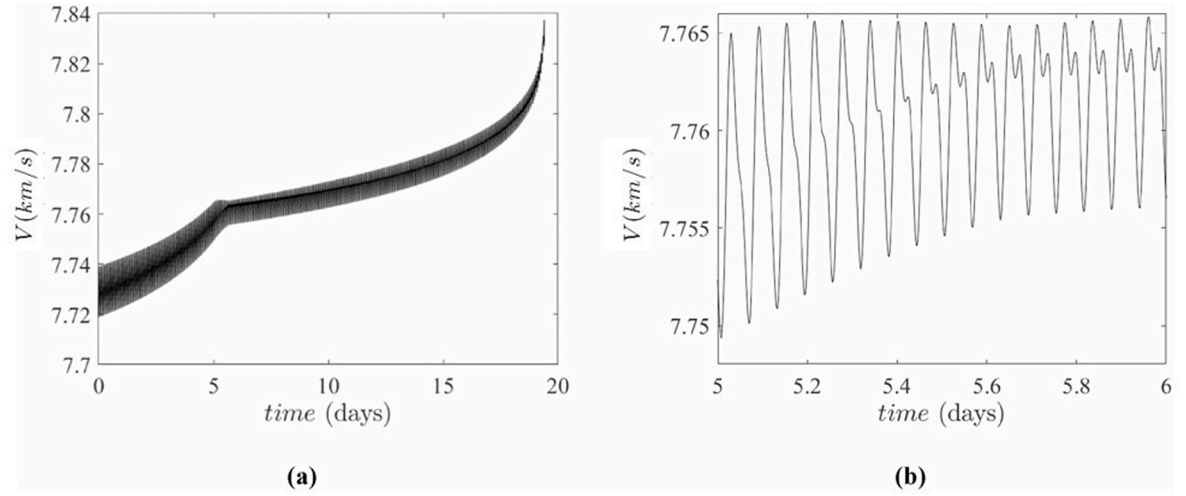

Fig. 14. Optimal profile of velocity (km/s) as function of time (a), with a zoom (b) to appreciate the oscillations.

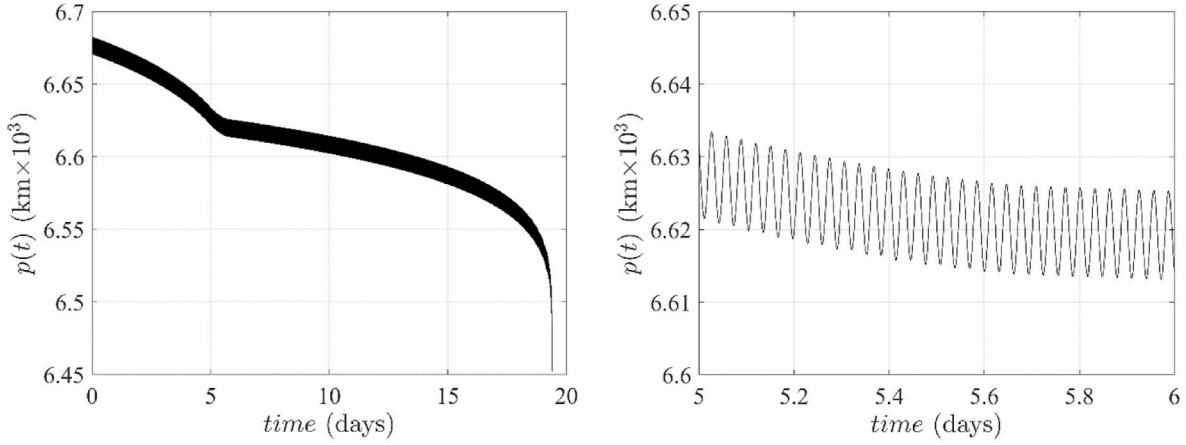

Fig. 15. Optimal profile of the p parameter (km x 10^3) as function of time (a), with a zoom (b) to appreciate the oscillations.

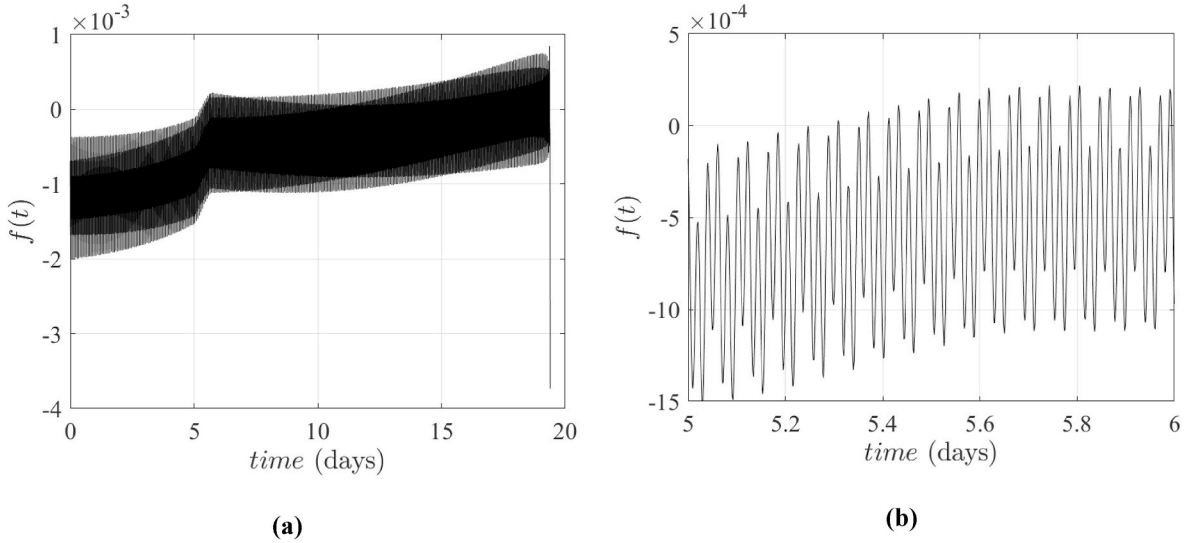

Fig. 16. Optimal profile of the f parameter as function of time (a), with a zoom (b) to appreciate the oscillations.

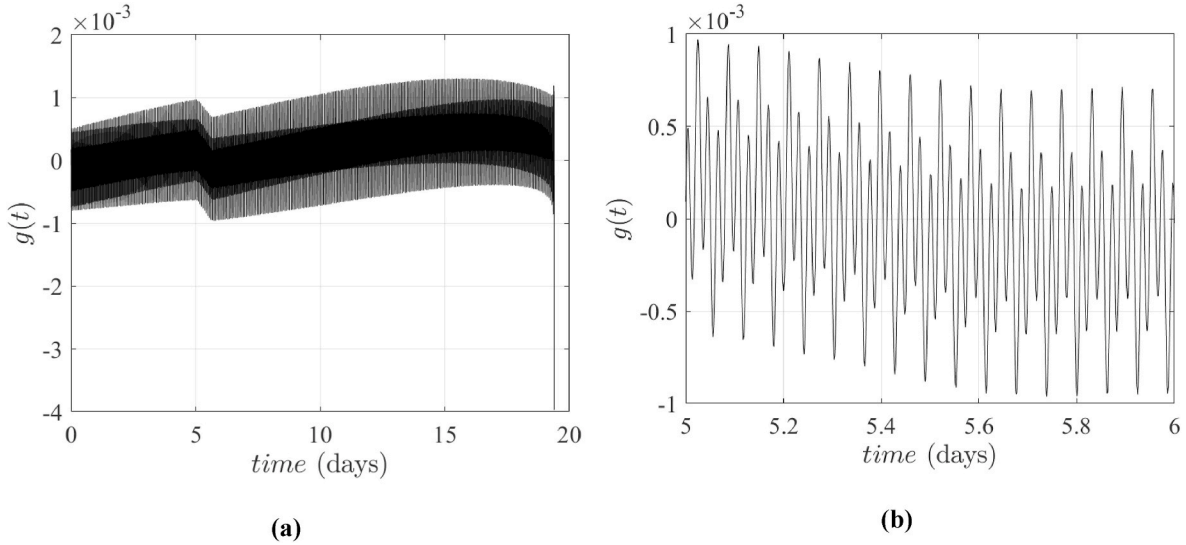

Fig. 17. Optimal profile of the g parameter as function of time (a), with a zoom (b) to appreciate the oscillations.

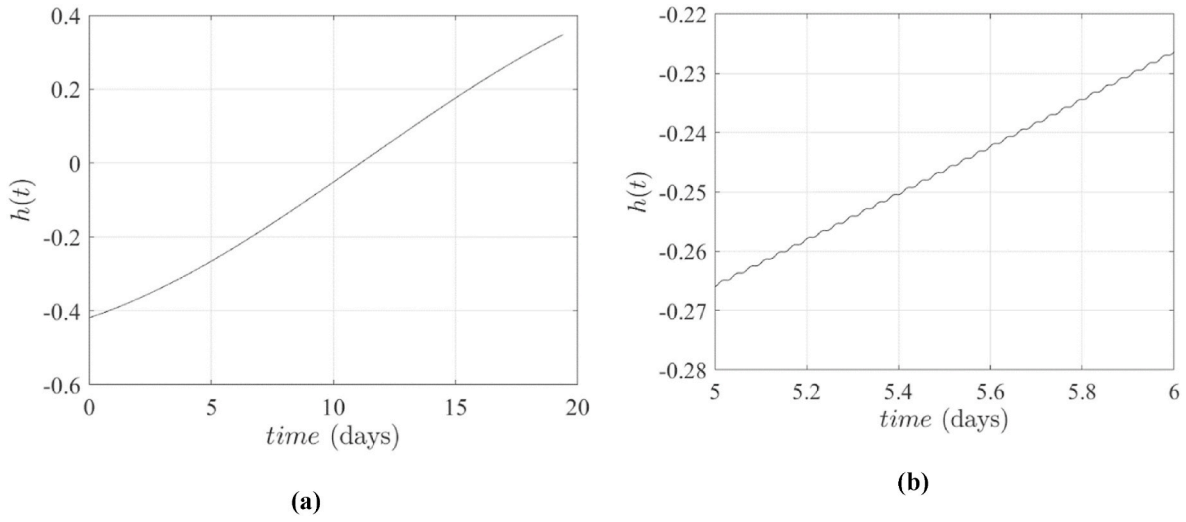

Fig. 18. Optimal profile of the h parameter as function of time (a), with a zoom (b) to appreciate the oscillations.

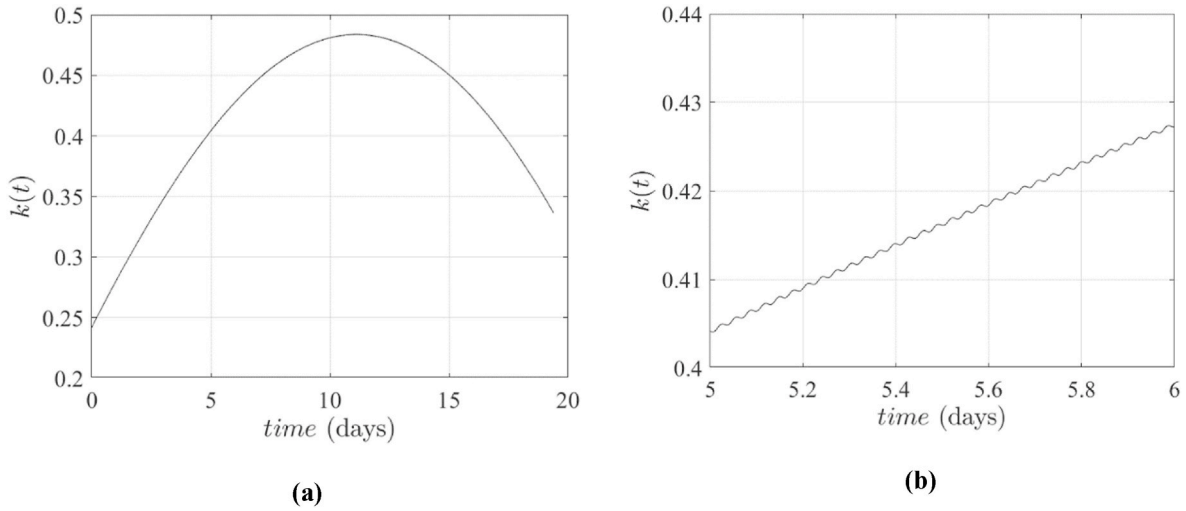

Fig. 19. Optimal profile of the k parameter as function of time (a), with a zoom (b) to appreciate the oscillations.

Table 5
Simulation initial conditions and satellite characteristics for the comparison between the two algorithms.

Simulation initial conditions and satellite characteristics for the comparison between algorithms	
a_0	6680 km
e_0	0.0007
i_0	51.84°
ω_0	10°
θ_0	20°
Ω_0	190°
m	40 kg
C_D	2
$[S_{min}; S_{max}]$	$[0.2\ m^2; 1.9\ m^2]$

maximum error on latitude and longitude is lower than 1.5%, the threshold imposed by the user. The successful outcome of the algorithm is testified by all resulting pairs included in this region.

The analysis showed the validity and robustness of the algorithm, further demonstrating its ability to successfully model a wide range of conditions. In addition, even if the maximum threshold imposed by the user is 1.5%, most of the longitude-latitude resulting pairs are characterized by an error of less than 0.5%, proving the high precision of the results.

Table 6
Parameters employed in Monte Carlo analysis.

Parameter	Range	Probability distribution
a	[6670 km; 6720 km]	Uniform
Ω	[0°; 360°]	Uniform
i	[30°; 70°]	Uniform
ω	[0°; 360°]	Uniform
e	[0; 0.001]	Uniform
θ	[0°; 360°]	Uniform
Epoch	[31st December 2017; 31st December 2022]	Uniform

5. Conclusions

This paper presents a novel algorithm to obtain minimum-time de-orbiting trajectories from a Low Earth Orbit (LEO) to a desired geo-location at re-entry interface. The formulation in terms of modified equinoctial orbital parameters and the independent variable change, from time to true longitude, managed the large time scale and the oscillatory nature of the problem. The problem is solved using a hp

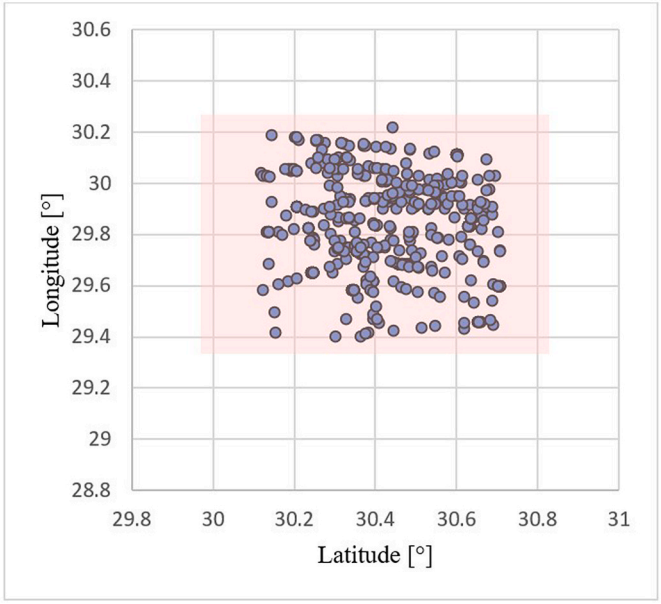

Fig. 20. Longitude-Latitude pairs resulting from the Monte Carlo analysis.

adaptive Gaussian quadrature orthogonal collocation method and formulated as a single-stage optimization problem. The objective is to find a surface profile to minimize the final time, defined as a terminal cost function. An event constraint on the altitude guaranteed its desired value at the re-entry interface. The algorithm application allows the assessment of the optimal control problem parameters ensuring the desired values of latitude and longitude. The novelty of this work lies in the identification of a common trend of solutions along an infinite-shaped pattern which allowed algorithm generalization and the possibility to model a wide range of missions, involving different initial conditions and satellites. In addition, the possibility to reach a desired geolocation at the re-entry interface in a minimum time makes the work even more innovative. A Monte Carlo analysis highlighted its robustness and validity, showing its successful outcome in a wide range of conditions. Some future applications of the algorithm could deal with the generation of open-loop optimal trajectories which could be combined with other techniques, i.e., Artificial Neural Networks (ANNs), to get closed loop control.

Declaration of competing interest

The authors declare that they have no known competing financial interests or personal relationships that could have appeared to influence the work reported in this paper.

Acknowledgements

This work is the result of a collaboration between Scuola Superiore Meridionale, Naples, Italy, and Embry-Riddle Aeronautical University (ERAU) Daytona Beach Campus, Florida, US. Authors would also like to acknowledge Scuola Superiore Meridionale for funding the travel abroad for Emanuela Gaglio, and Embry-Riddle Aeronautical University (ERAU) for hosting her for 12 months.

References

[1] R.P. Patera, W.H. Ailor, The realities of reentry disposal, Adv. Astronaut. Sci. 99 (1998) 1059–1071.
[2] R.P. Patera, W.H. Ailor, Spacecraft reentry strategies: meeting debris mitigation and ground safety requirements, Proc. IME G J. Aero. Eng. 221 (6) (2007) 947–953, https://doi.org/10.1243/09544100JAERO199.
[3] S.R. Omar, R. Bevilacqua, Hardware and GNC solutions for controlled spacecraft re-entry using aerodynamic drag, Acta Astronaut. 159 (2019) 49–64, https://doi.org/10.1016/j.actaastro.2019.03.051.
[4] D. Guglielmo, S.R. Omar, R. Bevilacqua, L. Fineberg, J. Treptow, B. Poffenberger, Y. Johnson, Drag deorbit device: a new standard reentry actuator for CubeSats, AIAA Journal of Spacecraft and Rockets 56 (1) (2019) 129–145, https://doi.org/10.2514/1.A34218.
[5] A. Fedele, S. Carannante, M. Grassi, R. Savino, Aerodynamic control system for a deployable re-entry capsule, Acta Astronaut. 181 (2021) 707–716, https://doi.org/10.1016/j.actaastro.2020.05.049.
[6] W. Okolo, B. Margolis, S.N. D'Souza, J. Barton, Pterodactyl: Development and Comparison of Control Architectures for a Mechanically Deployed Entry Vehicle, AIAA SciTech 2020 Forum, 2020, p. 2012, https://doi.org/10.2514/6.2020-1012.
[7] A. Alunni, S.N. D'Souza, B. Yount, W. Okolo, B. Nikaido, B. Margolis, B.J. Johnson, K. Hibbard, J. Barton, G. Lopez, Z.B. Hays, Pterodactyl: trade study for an integrated control system design of a mechanically deployed entry vehicle, in: AIAA SciTech 2020 Forum, 2020, p. 1014, https://doi.org/10.2514/6.2020-1014.
[8] E. Gaglio, R. Guida, A. Cecere, S. Mungiguerra, R. Savino, Assessment of a deployable aerodynamic control system for microsatellites recovery, in: 73rd *International Astronautical Congress*, 2022. Paris, FR.
[9] K. Pande, R. Venkatachalam, On optimal aerodynamic attitude control of spacecraft, Acta Astronaut. 6 (11) (1979) 1351–1359, https://doi.org/10.1016/0094-5765(79)90127-9.
[10] R. Ravindran, P.C. Hughes, Optimal aerodynamic attitude stabilization of near-Earth satellites, AIAA Journal of Spacecraft and Rockets 9 (7) (1972) 499–506, https://doi.org/10.2514/3.61730.
[11] M.L. Psiaki, Nanosatellite attitude stabilization using passive aerodynamics and active magnetic torquing, AIAA Journal of Guidance, Control, and Dynamics 27 (3) (2004) 347–355, https://doi.org/10.2514/1.1993.
[12] S.R. Omar, J.M. Wersinger, Satellite Formation Control using differential drag, in: *Proceedings of 53rd AIAA Aerospace Science Meeting*, 2014, https://doi.org/10.2514/6.2015-0002. Kissimmee, FL.
[13] D. Pérez, R. Bevilacqua, Differential drag-based reference trajectories for spacecraft relative maneuvering using density forecast, AIAA Journal of Spacecraft and Rockets 53 (1) (2016) 234–239, https://doi.org/10.2514/1.A33332.
[14] M. Pastorelli, R. Bevilacqua, S. Pastorelli, Differential-drag-based roto-translational control for propellant-less spacecraft, Acta Astronaut. 114 (2015) 6–21, https://doi.org/10.1016/j.actaastro.2015.04.014.
[15] C.L. Leonard, W.M. Hollister, E.V. Bergmann, Orbital formationkeeping with differential drag, AIAA Journal of Guidance, Control, and Dynamics 12 (1) (1989) 108–113, https://doi.org/10.2514/3.20374.
[16] Z.R. Putnam, R.D. Braun, Drag-modulation flight-control system options for planetary aerocapture, AIAA Journal of Spacecraft and Rockets 51 (1) (2013) 139–150, https://doi.org/10.2514/1.A32589.
[17] S. Varma, K.D. Kumar, Multiple satellite formation flying using differential aerodynamic drag, AIAA Journal of Spacecraft and Rockets 49 (2) (2012) 325–336, https://doi.org/10.2514/1.52395.
[18] R. Bevilacqua, M. Romano, Rendezvous maneuvers of multiple spacecraft using differential drag under J2 perturbation, AIAA Journal of Guidance, Control, and Dynamics 31 (6) (2008) 1595–1607, https://doi.org/10.2514/1.36362.
[19] N.X. Vinh, J.R. Johannesen, K.D. Mease, J.M. Hanson, Explicit guidance of drag-modulated aeroassisted transfer between elliptical orbits, AIAA Journal of Guidance, Control, and Dynamics 9 (3) (1986) 274–280, https://doi.org/10.2514/3.20103.
[20] M. Horsley, S. Nikolaev, A. Pertica, Small satellite rendezvous using differential lift and drag, AIAA Journal of Guidance, Control, and Dynamics 36 (2) (2013) 445–453, https://doi.org/10.2514/1.57327.
[21] A. Miele, 1st John V. Breakwell memorial lecture: recent advances in the optimization and guidance of aeroassisted orbital transfers, Acta Astronaut. 38 (10) (1996) 747–768, https://doi.org/10.1016/S0094-5765(96)00076-8.
[22] J. Virgili, P.C.E. Roberts, K. Palmer, S. Hobbs, J. Kingston, Descending sun-synchronous orbits with aerodynamic inclination correction, AIAA Journal of Guidance, Control, and Dynamics 38 (32) (2015) 831–842, https://doi.org/10.2514/1.G000183.
[23] J. Virgili, P.C.E. Roberts, N.C. Hara, Atmospheric interface reentry point targeting using aerodynamic drag control, AIAA Journal of Guidance, Control and Dynamics 38 (3) (2015) 403–413, https://doi.org/10.2514/1.G000884.
[24] S.R. Omar, R. Bevilacqua, D. Guglielmo, L. Fineberg, J. Treptow, S. Clark, Y. Johnson, Spacecraft deorbit point targeting using aerodynamic drag, AIAA Journal of Guidance, Control and Dynamics 40 (10) (2017) 1–7, https://doi.org/10.2514/1.G002612.
[25] S.R. Omar, R. Bevilacqua, Spacecraft de-orbit point targeting using aerodynamic drag, in: AIAA SciTech Forum, American Institute of Aeronautics and Astronautics, 2017.
[26] S.R. Omar, R. Bevilacqua, Guidance, navigation and control solutions for spacecraft re-entry point targeting using aerodynamic drag, Acta Astronaut. 155 (2019) 389–405, https://doi.org/10.1016/j.actaastro.2018.10.016.
[27] S. Dutta, A. Bowes, A.M. Dwyer Cianciolo, C. Glass, R.W. Powell, Guidance scheme for modulation of drag devices to enable return from Low Earth orbit, in: AIAA Atmospheric Flight Mechanics Conference, 2017, https://doi.org/10.2514/6.2017-0467. Paper 0467, Jan.
[28] R.A. Brouke, P.J. Cefola, On the equinoctial orbital elements, Celestial Mech. 5 (1972) 303–310, https://doi.org/10.1007/BF01228432.
[29] M.J.H. Walker, B. Ireland, J. Owens, A set of modified equinoctial orbital elements, Celestial Mech. 36 (1985) 409–419, https://doi.org/10.1007/BF01227493.

[30] G. Baù, J. Hernando-Ayuso, C. Bombardelli, A generalization of the equinoctial orbital elements, Celestial Mech. Dyn. Astron. 133 (2021) 1–29, https://doi.org/10.1007/s10569-021-10049-1.
[31] J.A. Kechichian, Equinoctial orbital elements: applications to optimal transfer problems, in: AIAA/AAS Astrodynamics Conference, 1990, https://doi.org/10.2514/6.1990-2976. Portland, OR, 20-22 August.
[32] J.T. Betts, Optimal interplanetary orbit transfers by direct transcriptions, J. Astronaut. Sci. 42 (3) (1994) 247–268.
[33] K.F. Graham, A.V. Rao, Minimum-time trajectory optimization of low-thrust earth-orbit transfers with eclipsing, AIAA Journal of Spacecraft and Rockets 53 (2) (2016) 289–303, https://doi.org/10.2514/1.A33416.
[34] H. Lui, B.H. Tongue, Indirect spacecraft trajectory optimization using modified equinoctial elements, AIAA Journal of Guidance, Control and Dynamics 33 (2) (2010) 619–623, https://doi.org/10.2514/1.45498.
[35] W. Wang, G. Mengali, A.A. Quarta, J. Yuan, Analysis of relative motion in non-Keplerian orbits via modified equinoctial elements, Aero. Sci. Technol. 58 (2016) 389–400, https://doi.org/10.1016/j.ast.2016.09.001.
[36] K.F. Graham, A.V. Rao, Minimum-time trajectory optimization of multiple revolution low-thrust Earth-orbit transfers, AIAA Journal of Spacecraft and Rockets 52 (3) (2015) 711–727, https://doi.org/10.2514/1.A33187.
[37] M.A. Patterson, A.V. Rao, GPOPS-II: a MATLAB software for solving multiple-phase optimal control problems using hp-adaptive Gaussian quadrature collocation methods and sparse nonlinear programming, ACM Trans. Math Software 41 (1) (2014), https://doi.org/10.1145/2684421, pp. 1:1 – 1:37.
[38] A.V. Rao, D.A. Benson, C.L. Darby, C. Francolin, M.A. Patterson, I. Sanders, G. T. Huntington, Algorithm 902: GPOPS, A matlab software for solving multiple-phase optimal control problems using the gauss pseudospectral method, ACM Trans. Math Software 37 (2) (2010), https://doi.org/10.1145/1731022.1731032. Article 22.
[39] D.A. Benson, G.T. Huntington, T.P. Thorvaldsen, A.V. Rao, Direct trajectory optimization and costate estimation via an orthogonal collocation method, AIAA Journal of Guidance, Control, and Dynamics 29 (6) (2006) 1435–1440, https://doi.org/10.2514/1.20478.
[40] G.T. Huntington, A.V. Rao, Optimal reconfiguration of tetrahedral spacecraft formations using the gauss pseudospectral method, AIAA Journal of Guidance, Control, and Dynamics 31 (3) (2008) 689–698, https://doi.org/10.2514/1.31083.